

Accurate Time-segmented Loss Model for SiC MOSFETs in Electro-thermal Multi-Rate Simulation

Jialin Zheng, *Student Member, IEEE*, Zhengming Zhao, *Fellow, IEEE*, Han Xu, *Student Member, IEEE*, Weicheng Liu, *Student Member, IEEE*, Yangbin Zeng, *Member, IEEE*

Abstract—Compared with silicon (Si) power devices, Silicon carbide (SiC) devices have the advantages of fast switching speed and low on-resistance. However, the effects of non-ideal characteristics of SiC MOSFETs and stray parameters (especially parasitic inductance) on switching losses need to be further evaluated. In this paper, a transient loss model based on SiC MOSFET and SiC Schottky barrier diode (SBD) switching pairs is proposed. The transient process analysis is simplified by time segmentation of the transient process of power switching devices. The electro-thermal simulation calculates the junction temperature and updates the temperature-related parameters with the proposed loss model and the thermal network model. A multi-rate data exchange strategy is proposed to solve the problem of disparity in timescales between circuit simulation and thermal network simulation. The CREE CMF20120D SiC MOSFET device is used for the experimental verification. The experimental results verify the accuracy of the model which provides guidance for the circuit design of SiC MOSFETs. All the parameters of the loss model can be extracted from the datasheet, which is practical in power electronics design.

Index Terms—Silicon Carbide (SiC) MOSFETs, power loss, electro-thermal, junction temperature.

I. INTRODUCTION

In recent years, SiC MOSFET devices have received more and more attention to meet the social demand of high efficiency and high power density in power electronics systems [1],[2]. Compared with Si devices of the same capacity, SiC devices have lower on-resistance, smaller junction capacitance, and can withstand higher operating junction temperatures. These advanced features result in lower device losses and higher switching speeds, which can improve the system efficiency and power density of power electronic converters [3]–[5]. SiC devices are increasingly used in high-power, high-voltage, and high-frequency applications, which necessitate higher efficiency and reliability.

Simulation is an effective way to analyze the efficiency and reliability of power electronic systems [6]–[10]. However, SiC devices are generally considered as ideal switches in the simulation of complex power converters, ignoring the delay and

distortion of the actual waveform during switching transient. This has led to a series of concerns. ① It is difficult to accurately analyze and simulate the destructive peak voltages and peak currents in transient processes, which threaten the safe operation of the devices. ② It is difficult to accurately calculate the switching loss and propose methods to reduce it. ③ It is difficult to account for the effect of junction temperature on the device parameters. Existing research results indicate that the change in the junction temperature of power devices is an important factor affecting their reliability and lifecycle [11]. Implementing simulations of power electronics converters that characterize SiC MOSFET switching transient loss and junction temperature variations plays a critical role in the assessment of device efficiency and reliability, as well as system-level modeling and engineering analysis. To achieve this goal, the transient loss model should be developed and used in electro-thermal simulation for junction temperature calculation.

The transient power losses can be calculated by two methods. The first method is the experimental fitting method, which obtains several sets of losses under different working conditions by experiment or datasheet, and fits to get the loss value of the required working condition [12]–[14]. Due to the obvious nonlinear characteristics of the SiC MOSFET, the accuracy of the losses obtained by this fitting is not sufficient. The second method is to calculate the losses by simulating the transient waveform of the device. The switching transient process of power switching devices is a complex coupling of multiple mechanisms of physical processes. There are two main types of modeling methods: physical models [15], [16] and behavioral models [17], [18]. The physical model is based on the physical theory of semiconductors, and mathematically expresses the internal mechanisms of the device and fundamentally constructs the physical model of the device. A representative is the McNutt model [15], which is highly accurate, but has large complexity, long simulation time, poor convergence, and is not suitable for engineering analysis. In [16], a PSpice physical model of SiC MOSFETs is developed, and the modeling focus is shifted from the internal mechanism of the device to the external characteristics, which has a shorter simulation time and

better convergence compared with [15], but still cannot meet the demand of system-level simulation.

The behavioral model is designed to simplify the analysis by segmenting the transient process according to the transient switching characteristics and the switching device state. In [17], the switching transient process of a power Si MOSFET is analyzed by using a time-segmented approach, but the model does not give an accurate analysis of the MOSFET turn-on current overshoot caused by the Schottky barrier diode (SBD) (reverse recovery process can be neglected) junction capacitance. In [18], a time segmentation approach is used to propose an analytical loss model of the converter based on SiC MOSFET and SiC SBD, but the model does not consider the effect of the nonlinear characteristics of C_{gd} on the transient process during the rapid change of v_{ds} and does not model the high frequency oscillation at the end of the transient process.

For the temperature characterization of the device, the RC thermal network or the finite element method (FEM) can be used for modeling. In [19], [20], an electrothermal model of power semiconductor devices based on electric-thermal field coupling was constructed in FEM software. Nevertheless, the lack of an accurate electrical model makes it difficult to accurately calculate the power losses of the device, which in turn affects the accuracy of the temperature field solution. In [21]–[24], RC thermal networks were introduced into electrical simulation platforms such as Spice and Saber through the concept of thermal-electrical analogy to construct an electro-thermal model based on electrical-thermal path coupling. This method is computationally more efficient than the FEM analysis method, but Saber and Spice simulations of transient circuits have the problems of slow simulation speed, small simulation circuit size, and poor convergence. In [25], A modeling method is proposed which used the switching pair as a basic unit and proposed a IGBT transient model.

A transient time-segmented loss model is proposed in this paper. The model can reflect the transient waveform and switching loss of the device more accurately and address the difficulty in extraction of physical parameters. This paper is organized as follows. Section II gives the parameters definition and description for the double-pulse test (DPT) circuit to analyze the transient loss of SiC MOSFET and SiC SBD switching pair. Section III proposes the time-segmented loss model and thermal model. Section IV introduces the electro-thermal simulation method based on the proposed loss model. The model proposed is validated in Section V by the operating characteristics of the double-pulse test circuit of Cree SiC MOSFET (CMF20120D) and SiC SBD (C4D30120D). The conclusion is drawn in Section VI.

II. MODEL DESCRIPTION OF SiC MOSFET AND SiC SBD SWITCHING CELL

In order to model the transients of SiC MOSFET and SiC SBD switching pair, this section uses a double-pulse test (DPT) circuit to analyze and model the transient process of SiC MOSFET in different stages. The parameters and descriptions for the DPT circuit are discussed in details as follows.

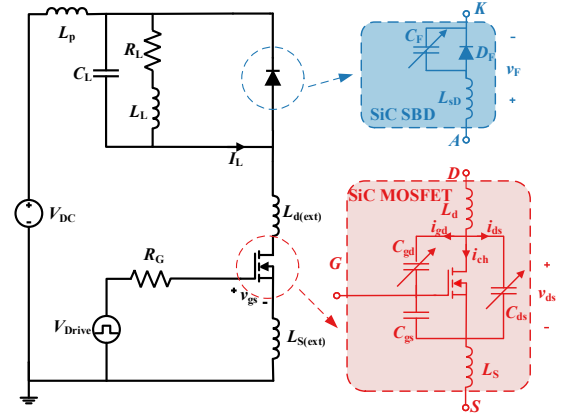


Fig. 1. Equivalent model of the double pulse testing circuit.

A. Parameters Definition

The DPT equivalent circuit model, which takes into account the stray parameters, is shown in Fig 1. The dc bus voltage is V_{DC} , the load inductance L_L is equivalent to the ideal current source I_L and the equivalent parallel capacitance is C_L , the output voltage V_{Drive} of the drive circuit is equivalent to an ideal square wave voltage source that jumps between the high-level V_{CC} and the low-level V_{EE} . R_g is the resistance of the driving circuit. L_p is the parasitic inductance of the dc bus.

For SiC MOSFET, the equivalent model includes ideal MOSFET, reflecting the static characteristics of SiC MOSFET; three parasitic capacitances, namely gate-source capacitance C_{gs} , gate-drain capacitance C_{gd} , and drain-source capacitance C_{ds} , which affect the transient characteristics of SiC MOSFET. L_d and L_s are drain and source stray inductances. Since the gate stray inductance is generally small, the effect on the transient waveform is not significant and can be ignored.

For SiC SBD, the model includes ideal diode D_F , reflecting the static characteristics of SiC SBD; parasitic junction capacitance C_F , which affects the transient characteristics of SiC SBD; series stray inductance L_{sD} , which can be ignored.

It should be noted that C_{gd} , C_{ds} , and C_F are non-linear capacitors. The capacitance of the above-mentioned nonlinear capacitors can be linearized piecewise in addition to the C_{gd} during the rapid change of v_{ds} to simplify nonlinearities[26]. Therefore, the capacitance can be divided into different values according to the voltage level, The parameter extraction method of nonlinear capacitance will be introduced in Section V.

Since L_{sD} can be ignored, the equivalent capacitance of the load inductance C_L is considered to be in parallel with the SiC SBD junction capacitance C_F . the equivalent junction capacitance of SBD $C_{F(eq)}=C_F+C_L$, the MOSFET input capacitance $C_{iss}=C_{gd}+C_{gs}$, and the output capacitance $C_{oss}=C_{gd}+C_{ds}$. The total stray inductance of the main loop $L_{stray}=L_s+L_d+L_p$.

B. DPT Circuit Description

The equivalent circuit can be quantitatively described by the following equations.

The KVL in the gate drive circuit:

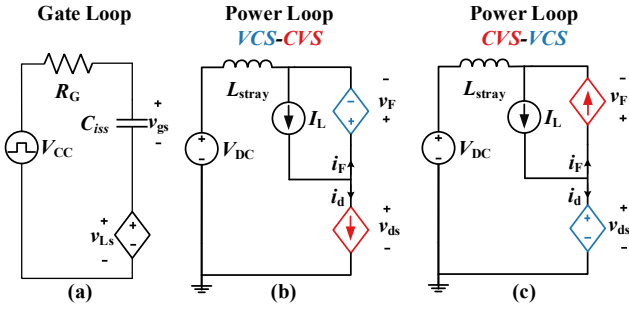


Fig. 2. Equivalent circuits during SiC MOSFET turn-on transition. (a) gate loop. (b) power loop-I. (c) power loop-II.

$$V_{\text{Drive}} = v_{C_{\text{iss}}}(t) + R_G i_g(t) + L_S \frac{di_d(t)}{dt} \quad (1)$$

where V_{Drive} has two values. When the MOSFET is turning on, its value is V_{CC} ; When the MOSFET is turning off, its value is V_{EE} , i_g is the current in the gate loop, i_d is the MOSFET drain current.

The KCL in the gate drive circuit:

$$i_g(t) = C_{gs} \frac{dv_{gs}(t)}{dt} + C_{gd} \frac{dv_{gd}(t)}{dt}. \quad (2)$$

where v_{gs} is the gate-source voltage of SiC MOSFET, v_{gd} is the gate-drain voltage of SiC MOSFET, v_{ds} is the gate-drain voltage of SiC MOSFET.

The voltage relationship between capacitors:

$$v_{gs}(t) = v_{gd}(t) + v_{ds}(t). \quad (3)$$

The KVL in the DPT circuit:

$$V_{DC} = v_{ds}(t) + L_{stray} \frac{di_d}{dt} - v_F \quad (4)$$

where v_F represents the voltage drop on the SBD,

$$\begin{cases} v_F = v_{F0} & \text{SBD on} \\ i_{\text{Diode}} = -C_{F(\text{eq})} \frac{dv_F}{dt} & \text{SBD off.} \end{cases} \quad (5)$$

The KCL in the DPT circuit:

$$i_L(t) = i_F(t) + i_d(t) \quad (6)$$

$$i_d(t) = i_{ch}(t) + i_{gd}(t) + i_{ds}(t) \quad (7)$$

where i_F is the current through SBD, i_{ch} is determined by v_{gs} and v_{ds} ,

$$i_{ch}(t) = \begin{cases} g_{fs} [v_{gs}(t) - V_{th}] & v_{gs} > V_{th}, v_{ds} > v_{gs} - V_{th} \\ 0 & v_{gs} \leq V_{th} \\ v_{ds}(t) / R_{on} & v_{gs} > V_{th}, v_{ds} \leq v_{gs} - V_{th} \end{cases} \quad (8)$$

where g_{fs} is the linearized transconductance (A/V); V_{th} is the linearized threshold voltage; $R_{ds(\text{on})}$ is the on-state resistance.

The differential equations composed of (1)-(8) are difficult to solve directly. To reduce the calculation, this paper proposed a transient time-segmented model to represent the transient behavior of the switching device in Fig 1. The proposed model is detailed in Section III.

III. ELECTRO-THERMAL MODEL OF SiC MOSFET AND SiC SBD SWITCHING PAIR

The electro-thermal model is divided into two parts to

describe the electrical and thermal behavior of SiC MOSFET and SBD: The electrical model is used to calculate the losses of the MOSFET and SBD. The thermal model is used to calculate the device temperature and to modify the temperature-related parameters of the electrical model according to the temperature.

The total power losses of SiC MOSFET and SBD mainly includes two parts: conduction loss and switching loss. The conduction loss is easy to calculate and will not be described in detail here. This section mainly describes the loss and electrical behavior of MOSFET and SBD during the turn-on and turn-off process. The thermal modeling method and the temperature correction of the parameters are also explained in this section.

The equivalent model of DPT is decoupled to gate loop and power loop shown in Fig 2. The power loop is divided into two modes, CVS-VSC and VCS-CVS, according to the behavior of MOSFETs and SBDs.

A. Gate Loop Analysis

The time duration of the following stage can be calculated by analyzing the gate loop shown in Fig 2 (a). The voltage of the L_S can be used as a controlled source to decouple the control loop from the power loop.

$$v_{L_S} = L_S \frac{di_d(t)}{dt} \quad (9)$$

Gate loop power supply V_{drive} controls the on/off of the MOSFET by charging and discharging C_{iss} through R_G . The voltage relationship in the gate loop can be expressed as

$$V_{\text{Drive}} = R_G i_g + v_{C_{\text{iss}}} + v_{L_S} \quad (10)$$

where $v_{C_{\text{iss}}}$ represents the voltage on the capacitance C_{iss} .

The current of the control loop charges and discharges C_{iss} . According to (2) and (3), the relationship of the currents can be expressed as

$$i_g = C_{\text{iss}} \frac{dv_{gs}(t)}{dt} - C_{gd} \frac{dv_{ds}(t)}{dt}. \quad (11)$$

B. Turn-on Power Loop Analysis

The SiC MOSFET and SiC SBD switching loss can be calculated as

$$E_{\text{loss}}(\text{MOS}) = \int v_{ds}(t) \cdot i_d(t) dt \quad (12)$$

$$E_{\text{loss}}(\text{SBD}) = \int v_F(t) \cdot i_F(t) dt$$

where $E_{\text{loss}}(\text{MOSFET})$ represents the loss energy produced by SiC MOSFET, $E_{\text{loss}}(\text{SBD})$ represents the loss energy produced by SiC SBD. The analytical expressions $v_{ds}(t)$, $i_d(t)$, $v_F(t)$ and $i_F(t)$ describing the behavior of SBD and MOSFET are related to the turn-on process, which is divided into multiple stages.

A typical SiC MOSFET turn-on transient waveform is shown in Fig 3. The turn-on transient process can be divided into 8 stages. Table I lists the time duration, the current and voltage expression of SiC MOSFET and SiC SBD, and the loss expressions for each stage in the turn-on process. The specific expressions of each stage are introduced in Appendix A.

Stage 1 (t_1 - t_2): This is C_{iss} charging stage, The output voltage V_{drive} rises from V_{EE} to V_{CC} at t_1 , and v_{gs} starts to rise. v_{gs} rises to V_{th} at t_2 . the drive circuit starts to charge the MOSFET input capacitance C_{iss} at t_1 . Since L_S is small and the rate of change of

TABLE I
TURN-ON PROCESS

Stage	Time Duration	Analytical Expression of SBD and MOSFET	Loss Expression of SBD and MOSFET
t_1-t_2	$t_2-t_1 = R_G C_{iss} \ln\left[\frac{(V_{CC}-V_{EE})}{(V_{CC}-V_{th})}\right]$	$\begin{cases} i_d = 0, & v_{ds} = v_{F(on)} + V_{DC} \\ i_F = I_L, & v_F = v_{F0} \end{cases}$	$\begin{cases} E_{loss}(\text{MOS}) = 0 \\ E_{loss}(\text{SBD}) = I_L v_{F0} (t_2 - t_1) \end{cases}$
t_2-t_3	$t_3-t_2 = \frac{B + \sqrt{(B^2 - 4AC)}}{2A}$ $A = (V_{CC} - (V_{gs}(t_3) + V_{th}) / 2)$ $B = R_G C_{iss} (V_{gs}(t_3) - V_{th}) + L_{stary} (I_L / 2)$ $C = R_G C_{gd} L_{stary} I_L / 2$	$\begin{cases} i_d(t) = a_{23}(t-t_2)^3 + b_{23}(t-t_2)^2 + c_{23}(t-t_2) + d_{23} \\ v_{ds}(t) = V_{DC} + v_F - L_{stary} \frac{di_d(t)}{dt} \\ i_F(t) = I_L - i_d(t), & v_F(t) = v_{F0} \end{cases}$	$\begin{cases} E_{loss}(\text{MOS}) = (V_{DC} + v_F) \int_{t_2}^{t_3} i_d(t) dt - \frac{1}{2} L_{stary} i_d^2(t) \Big _{t_2}^{t_3} \\ E_{loss}(\text{SBD}) = v_{F0} I_L (t_3 - t_2) - v_{F0} \int_{t_2}^{t_3} i_d(t) dt \end{cases}$
t_3-t_4	$t_4-t_3 = \frac{\left[R_G C_{iss} (V_{miller} - V_{gs}(t_3)) + L_{stary} (I_L / 2) \right]}{(V_{CC} - (V_{miller} + V_{gs}(t_3)) / 2)}$	$\begin{cases} i_d(t) = i_d(t) = \frac{I_L}{2(t_4 - t_3)} (t - t_3) + \frac{I_L}{2}, & v_{ds}(t) = V_{ds0} \\ i_F(t) = I_L - i_d(t), & v_F(t) = v_{F0} \end{cases}$	$\begin{cases} E_{loss}(\text{MOS}) = \frac{3}{4} V_{ds0} I_L (t_4 - t_3) \\ E_{loss}(\text{SBD}) = \frac{1}{4} (V_{DC} - V_{ds0}) I_L (t_4 - t_3) \end{cases}$
t_4-t_5	$t_5-t_4 = \frac{\left[R_G C_{iss} (V_{gs_peak} - V_{miller}) + L_{stary} (I_{peak} - I_L) \right]}{(V_{CC} - (V_{gs_peak} + V_{miller}) / 2)}$	$\begin{cases} i_d(t) = a_{45}(t-t_4)^3 + b_{45}(t-t_4)^2 + c_{45}(t-t_4) + d_{45} \\ v_{ds}(t) = V_{ds0}, & i_F(t) = I_L - i_d(t) \\ v_F(t) = V_{ds0} - V_{DC} + L_{stary} \frac{di_d(t)}{dt} \end{cases}$	$\begin{cases} E_{loss}(\text{MOS}) = V_{ds0} C_{F(eq)} (V_{DC} + v_F - V_{ds0}) + I_L V_{ds0} (t_5 - t_4) \\ E_{loss}(\text{SBD}) = (V_{DC} - V_{ds0}) C_{F(eq)} (V_{DC} + v_F - V_{ds0}) - \\ \frac{1}{2} L_{stary} i_d^2(t) \Big _{t_4}^{t_5} - I_L V_{ds0} (t_5 - t_4) + L_{stary} I_L i_d(t) \Big _{t_4}^{t_5} \end{cases}$
t_5-t_6	$t_6-t_5 = \frac{[-R_G C_{gd} (V_{miller} - V_{th} - V_{ds0})]}{(V_{CC} - V_{miller})}$	$\begin{cases} i_d = I_L + I_{os} e^{-\alpha_{on}(t-t_5)} \cos(\omega_{on}(t-t_5)) \\ i_F(t) = I_L - i_d(t) \end{cases}$	$\begin{cases} E_{loss}(\text{MOS}) = I_L V_{ds(av)} (t_8 - t_5) + I_{os} \frac{\alpha_{on}}{\alpha_{on}^2 + \omega_{on}^2} V_{ds(av)} \\ E_{loss}(\text{SBD}) = (V_{DC} - V_{ds(av)}) I_{os} \frac{\alpha_{on}}{\alpha_{on}^2 + \omega_{on}^2} - \\ \frac{1}{2} L_{stary} (i_d(t) - I_L)^2 \Big _{t_5}^{t_8} \end{cases}$
t_6-t_7	$t_7-t_6 = \frac{-R_G C_{gd} (V_{ds(on)} - (V_{miller} - V_{th}))}{(V_{CC} - V_{miller})}$	$\begin{cases} v_F(t) = v_{ds}(t) - V_{DC} + L_{stary} di_d(t)/dt \\ v_{ds}(t) = \frac{(V_{t_end} - V_{t_start})}{(t_{end} - t_{start})} (t - t_{start}) + V_{start}, t_{start} \leq t < t_{end} \end{cases}$	
t_7-t_8	$t_8-t_7 \approx 2R_G C_{iss}$		

the current flowing through L_s is small, the L_s voltage v_{Ls} equals zero.

The expression of the gate-source voltage v_{gs} in this stage is

$$v_{gs}(t) = V_{CC} + (V_{EE} - V_{CC}) \exp\left(-\frac{t-t_1}{R_G C_{iss}}\right). \quad (13)$$

Stage 2&3 (t_2-t_3): This is the current rising stage. In this stage, v_{gs} starts to rise from V_{th} to V_{miller} , MOSFET enters the saturation region. i_d starts to rise from 0 to I_L , and v_{ds} starts to fall from $V_{DC}+v_F$. Due to the stray inductance voltage drop $L_{stary}|di_d/dt|$ and the non-linearity of the SBD junction capacitance C_F , v_{ds} will remain unchanged when it drops to a certain value V_{ds0} . To simplify the analysis, this paper assumes that v_{ds} is V_{ds0} when the current rises to $I_L/2$. Therefore, this stage will be divided into two stages.

Stage 2 (t_2-t_3): This is the current rising sub-stage I. In this stage, i_d starts to rise from 0 to $I_L/2$, v_{gs} rises from V_{th} to $V_{gs}(t_3)$. v_{ds} drops from $V_{DC}+v_F$ to V_{ds0} , V_{drop} is the difference between $V_{DC}+v_F$ and V_{ds0} .

Stage 3 (t_3-t_4): This is the current rising sub-stage II. In this stage, v_{ds} keeps V_{ds0} and i_d starts to linear rise from $I_L/2$ to I_L . v_{gs} rises from $V_{gs}(t_3)$ to V_{miller} .

Stage 4 (t_4-t_5): This is the current rising stage III. At t_4 , the MOSFET current i_d rises to I_L , the SBD current i_F drops to 0, and the SBD turns off. Although the reverse recovery process of SiC SBD is negligible, the i_d overshoots due to the reverse voltage and reverse charging of its junction capacitance. i_d starts to rise from I_L to I_{peak} , v_{ds} keeps V_{ds0} . v_{gs} rises from V_{miller} to V_{gs_peak} .

Stage 5 (t_5-t_6): This is the voltage falling stage I. v_{ds} drop from

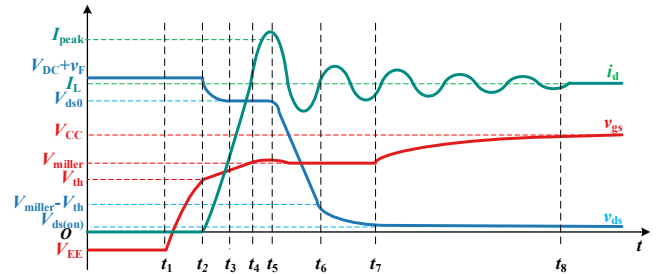


Fig. 3. Turn-on transient waveforms of SiC MOSFET.

V_{ds0} to $V_{miller}-V_{th}$ linearly. v_{gs} is approximately V_{miller} and remains unchanged.

Stage 6 (t_6-t_7): This is the voltage falling stage II. The gate-drain voltage v_{ds} drop from $V_{miller}-V_{th}$ to $V_{ds(on)}$ linearly, v_{gs} remains approximately V_{miller} .

Stage 7 (t_7-t_8): This is the voltage falling stage III. The gate-drain voltage v_{ds} keeps as $V_{ds(on)}$, The gate-source voltage v_{gs} rises from V_{miller} to V_{CC} exponentially.

Current Oscillation Stage (t_5-t_8): The drain current of MOSFET i_d enters the oscillation stage from t_5 due to the L_{stary} and C_F .

In summary, the time durations of each stage can be obtained through (1) and (2), that is, to solve the (10) and (11).

C. Turn-off Power Loop Analysis

The typical turn-off transient waveform of SiC MOSFET is shown in Fig 4. The turn-off process is the inverse process of the turn-on process. The turn-off transient process can be divided into 5 stages. The time durations, the state expressions

TABLE II
TURN-OFF PROCESS

Stage	Time Duration	Analytical Expression of SBD and MOSFET	Loss Expression of SBD and MOSFET
t_1-t_2	$t_2-t_1 = R_G C_{iss} \ln[(V_{CC} - V_{EE}) / (V_{CC} - V_{th})]$	$\{i_d = I_L, v_{ds} = V_{ds(on)}, i_F = 0, v_F = -V_{DC} - V_{ds(on)}\}$	$\{E_{loss}(\text{MOS}) = I_L V_{ds(on)} (t_2 - t_1), E_{loss}(\text{SBD}) = 0\}$
t_2-t_3	$t_3-t_2 = R_G C_{gd} \frac{(V_{miller} - V_{th} - V_{ds(on)})}{(V_{miller} - V_{EE})}$	$\begin{cases} i_d(t) = I_L, v_{ds}(t) = \frac{V_{miller} - V_{th} - V_{ds(on)}}{t_3 - t_2} (t - t_2) + V_{ds(on)} \\ i_F(t) = 0, v_F(t) = V_{DC} - v_{ds}(t) \end{cases}$	$\begin{cases} E_{loss}(\text{MOS}) = \frac{(V_{miller} - V_{th} + V_{ds(on)})}{2} I_L (t_3 - t_2) \\ E_{loss}(\text{SBD}) = 0 \end{cases}$
t_3-t_4	$t_4-t_3 = \left[\frac{R_G C_{iss} (V_{gs}(t_4) - V_{miller}) - R_G C_{gd} \Delta V_{ds1} + L_{stray} (I_{t4} - I_L)}{(V_{EE} - (V_{gs}(t_4) + V_{miller}) / 2)} \right]$	$\begin{cases} i_F(t) = C_{F(eq)} \frac{dv_{ds}(t)}{dt}, v_{ds}(t) = \frac{\Delta V_{ds}}{t_4 - t_3} (t - t_3) + V_{miller} - V_{th} \\ i_d(t) = I_L - C_{F(eq)} \frac{dv_{ds}(t)}{dt}, v_F(t) = -V_{DC} + v_{ds}(t) + L_{stray} \frac{di_d(t)}{dt} \end{cases}$	$\begin{cases} E_{loss}(\text{MOS}) = \frac{(I_L + I_{t4}) (V_{miller} - V_{th} + V_{DC})}{2} (t_4 - t_3) \\ E_{loss}(\text{SBD}) = \frac{-(I_L - I_{t4})}{2} \left(V_{DC} - \frac{(V_{miller} - V_{th} + V_{DC})}{2} (t_4 - t_3) \right) \end{cases}$
t_6-t_7	$t_7-t_6 = \frac{I_{t6} L_{stray} + R_G C_{iss} (V_{miller3} - V_{th})}{(0.5V_{miller} + 0.5V_{miller3} - V_{EE})}$	$\begin{cases} i_d(t) = \frac{-I_{t6}}{t_7 - t_6} (t - t_6) + I_{t6}, v_{ds}(t) = V_{DC} + V_{OS} \cos(\omega_{off} (t - t_6)) \\ i_F(t) = I_L - i_d(t), v_F(t) = -V_{DC} + v_{ds}(t) + L_{stray} \frac{di_d(t)}{dt} \end{cases}$	$\begin{cases} E_{loss}(\text{MOS}) = \frac{I_{t6}}{2} \left(V_{DC} + \frac{2V_{OS}}{\pi} \right) (t_7 - t_6) \\ E_{loss}(\text{SBD}) = \left(I_L - \frac{I_{t6}}{2} \right) V_{F0} (t_7 - t_6) \end{cases}$
t_7-t_8	$t_8-t_7 \approx 2R_G C_{iss}$	$\begin{cases} i_d(t) = C_{oss} dv_{ds}(t) / dt \\ v_{ds}(t) = V_{DC} + v_{F0} + V_{OS} e^{-\alpha_{off}(t-t_7)} \cos(\omega_{off}(t-t_7)) \\ i_F(t) = I_L - i_d(t), v_F(t) = v_{F0} \end{cases}$	$\begin{cases} E_{loss}(\text{MOS}) = -C_{oss} V_{OS} (V_{DC} + v_{F0}) + V_{OS} I_L \frac{\alpha_{off}}{\alpha_{off}^2 + \omega_{off}^2} \\ E_{loss}(\text{SBD}) = I_L V_{F0} (t_8 - t_7) + C_{oss} V_{OS} v_{F0} \end{cases}$

of the switching device, and the loss expressions in each stage are shown in Table II. The specific expressions of each stage are introduced in Appendix A.

Stage 1 (t_1-t_2): This is C_{iss} discharging stage, v_{gs} drops from V_{CC} to V_{miller} . At this stage, the MOSFET is in the linear zone. Neither v_{ds} nor i_d will change. At t_2 , v_{gs} drops to V_{miller} .

Stage 2 (t_2-t_3): This is voltage rising stage I. v_{ds} slowly rises from $V_{ds(on)}$ to $V_{miller} - V_{th}$, v_{gs} remains approximately as V_{miller} . The SBD is cut-off in this stage, v_{ds} and v_F change slowly, and the SBD junction capacitance current i_{Diode} can be neglected. Therefore, i_d remains approximately as I_L in this stage.

Stage 3 (t_3-t_4): This is voltage rising stage II. the MOSFET enters the saturation region, and v_{ds} rises rapidly. During this stage, v_F drops rapidly, and the SBD junction capacitance discharge current i_{Diode} cannot be ignored, which leads to a slow drop in i_d . It is approximately regarded as $d v_F / dt = -d v_{ds} / dt$, and i_d can be expressed as

$$i_d(t) = I_L - C_{F(eq)} \frac{d v_{ds}(t)}{dt}. \quad (14)$$

v_{ds} rises from $V_{miller} - V_{th}$ to V_{DC} , $\Delta V_{ds1} = V_{DC} - (V_{miller} - V_{th})$. i_d drops from I_L to I_{t4} , v_{gs} decreases from V_{miller} to $V_{gs}(t_4)$ due to i_d falling.

Stage 4 (t_4-t_5): v_{ds} rises to $V_{DC} + v_{F0}$ at t_6 . Due to the rapid decline of i_d through inductance L_{stray} , v_{ds} is overmodulated to the peak value V_{peak} . i_d drops from I_{t6} to 0, v_{gs} decreases from $V_{gs}(t_6)$ to V_{th} .

Stage 5 (t_5-t_6): v_{gs} drops to V_{th} at t_6 and continue to decline exponentially to V_{EE} . The MOSFET enters the cut-off region. It is considered that the SBD starts to conduct at this moment. v_{ds} and i_d come into oscillation stage.

D. Thermal Model and Parameters Correction

The thermal network is the key module to convert the power loss of the SiC MOSFET into the junction temperature of the device. Fig 5 shows the I - D equivalent thermal network model

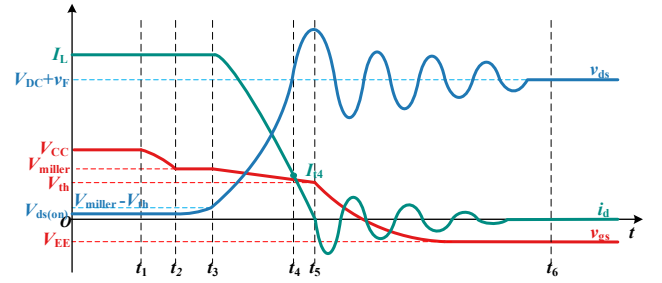


Fig. 4. Turn-off transient waveforms of SiC MOSFET.

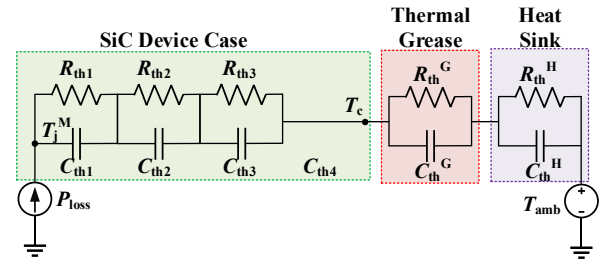


Fig. 5. Thermal calculation circuit of the power electronics device.

of the SiC MOSFET and SBD. The SiC MOSFET conducts heat conduction from the PN junction to the external environment T_{amb} . The power loss passes through the thermal network from the case to the external environment to obtain the case temperature T_c , and then passes through the PN junction to the thermal network of the substrate to obtain the junction temperature T_j . The temperature T_j of MOSFET and SBD can be expressed as

$$T_j = P_{loss} \sum_{i=1}^4 \left(\frac{R_{th}(i)}{R_{th}(i) C_{th}(i) + 1} \right) + T_c \quad (15)$$

$$T_c = P_{loss} (Z_{th}^G + Z_{th}^H) + T_{amb}.$$

The change of junction temperature T_j has a great influence on the value of electrical parameters. The influence of T_j on the

characteristics of SiC MOSFET and SiC SBD is mainly manifested in the influence on threshold voltage V_{th} , transconductance coefficient k , and on-resistance $R_{ds(on)}$. The relationship can be expressed as

$$V_{th} = V_{th0} + a(T_j - T_0) \quad (16)$$

$$k_{fs} = k_0 + b(T_j - T_0) \quad (17)$$

$$R_{ds(on)} = R_{ds(on)0} (cT_j^2 + dT_j + e) \quad (18)$$

where a-e are coefficients and can be obtained by the curve fitting method.

It is noted that the linear transconductance g_{fs} and threshold voltage V_{th} can be derived as

$$g_{fs} = \frac{2(\lambda^2 + 3\lambda + 3)}{3\lambda(1 + \lambda)} \sqrt{k_{fs} I_L}, \lambda = \sqrt{6} \quad (19)$$

$$V_{th} = \sqrt{I_L / k_{fs}} / (1 + k_{fs}) + V_{th0}$$

In addition, since the temperature has a small influence on the capacitance between electrodes, the correlation between the capacitance and temperature is not considered here.

IV. ELECTRO-THERMAL SIMULATION BASED ON TIME-SEGMENTED LOSS MODEL

A. Electro-thermal simulation Strategy

The relationship between the electrical model and thermal model of transient switching pair (TSP) can be expressed as follow, as shown in Fig 6. The power losses generated by MOSFET lead to an increase in module temperature, and the temperature changes affect the electrical characteristics of the MOSFET. Therefore, loss and temperature parameters are an important bridge between electrical and thermal simulations. The two models are coupled electrically and thermally by the mutual transfer of temperature and loss. The large difference in the timescales of the two models is a challenge for the interaction of loss and temperature data.

B. Data exchange between loss model and thermal model

An adaptive data exchange strategy is proposed to solve the problem of disparity in timescales between circuit simulation (ns) and thermal network simulation (ms). The adaptive step $dt_{th}(i)$ is adjusted according to the temperature change $dT(i)$ calculated in the previous step.

$$dt_{th}(i) = t_{th}(i) - t_{th}(i-1) \quad (20)$$

$$dT_{th}(i) = T_{th}(i) - T_{th}(i-1) \quad (21)$$

Temperature exceeding the upper threshold is defined as an event. When the temperature rises, if the temperature rise $dT(i)$ does not exceed the upper threshold, $dt_{th}(i)$ continuously increases by a constant ξ . If $dT(i)$ exceeds the upper threshold, i.e., the thermal-level event occurs, $dt_{th}(i)$ maintains the previous step size.

$$\begin{cases} dT_{th}(i) - dT_{th}(i-1) \leq \Delta T \Rightarrow dt_{th}(i) = dt_{th}(i-1) + \xi \\ dT_{th}(i) - dT_{th}(i-1) > \Delta T \Rightarrow dt_{th}(i) = dt_{th}(i-1) \end{cases} \quad (22)$$

The temperature drop to the lower threshold is defined as another event. As the temperature drops, $dt_{th}(i)$ first changes back to the minimum step size. If $dT(i)$ does not exceed the

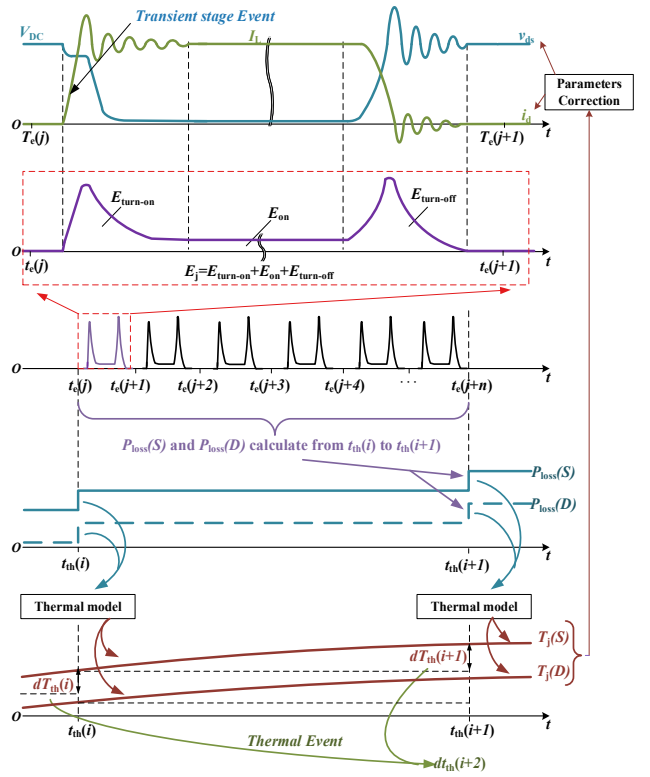


Fig. 6. Proposed electro-thermal simulation overview.

lower threshold, $dt_{th}(i)$ continuously increases by a constant ξ . If the $dT(i)$ exceeds the lower threshold, the thermal-level event occurs and $dt_{th}(i)$ remains the same as the previous step.

$$\begin{cases} dT_{th}(i) < 0, dT_{th}(i-1) < 0 \Rightarrow dt_{th}(i) = dt_{th}(i-1) \\ \begin{cases} dT_{th}(i) - |dT_{th}(i-1)| \leq \Delta T \Rightarrow dt_{th}(i) = dt_{th}(i-1) + \xi \\ |dT_{th}(i) - |dT_{th}(i-1)|| > \Delta T \Rightarrow dt_{th}(i) = dt_{th}(i-1) \end{cases} \end{cases} \quad (23)$$

With the same simulation accuracy, the adaptive time step increases the simulation efficiency by adjusting the simulation step according to the rate of temperature change, although it increases the complexity compared to a fixed step. The cost of this adaptive step management is that the power loss must be averaged over the circuit simulation time, as shown in Fig 6, due to the large difference in time scales between the device level simulation and the thermal simulation. As such, very small thermal transients (e.g., temperature fluctuations due to a single switching event) will be ignored.

It should be noted that the step size $dt_{th}(i)$ affects the temperature variation $dT(i)$, which has an impact on the device the electrical behavior. Therefore, a reasonable temperature variation threshold requires to be set, and the temperature variation threshold ΔT set in this paper is 1°C.

V. EXPERIMENT VERIFICATION

A. Experiment Parameters Extraction

The DPT platform is shown in Fig 7. The SiC MOSFET (CMF20120D) and SiC SBD (C4D30120D) from Wolfspeed are used as examples for the following experimental verification[27], [28]. The method of extracting the transient

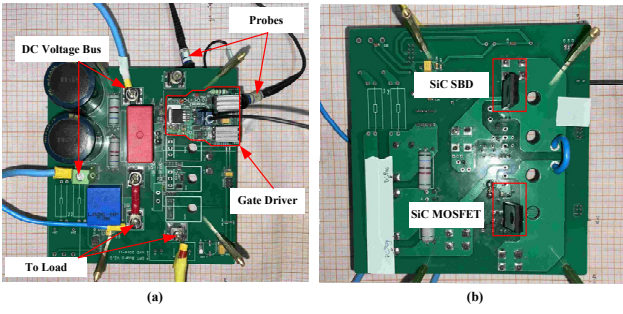


Fig. 7. The double pulse test circuit. (a) Top view. (b) Bottom view.

model parameters of SiC MOSFET and SiC SBD based on the datasheet is given as follows and their values are shown in Table III. The parameters to be extracted in the SiC MOSFET model include threshold voltage V_{th} , transconductance g_{fs} , parasitic capacitance C_{gs} , C_{gd} , and C_{ds} .

The threshold voltage V_{th} and transconductance g_{fs} can be obtained from the transfer characteristic curves of SiC MOSFET. The channel current i_{ch} and the gate-source voltage v_{gs} satisfies the relationship

$$i_{ch} = k_{fs} (v_{gs} - v_{th0})^2 \quad (24)$$

where k_{fs} and v_{th0} can be obtained by fitting the transfer characteristic curve of the datasheet.

The MOSFET transfer characteristic curve is linearized at $i_{ch}=I_L/2$ and replaced by a tangent line to simplify the analysis. The linearization relationship between channel current i_{ch} and the gate-source voltage v_{gs} is shown in (8). The threshold voltage V_{th} and transconductance g_{fs} can be calculated from k_{fs} and v_{th0} using (19).

The gate source capacitance C_{gs} is the gate oxide layer capacitance, and its capacitance can be approximated as a constant due to the constant oxide layer thickness; the segmented capacitance values reflect the nonlinearity of the parasitic capacitance C_{ds} and C_{gd} to facilitate the calculation. The extraction method of the SBD junction capacitance C_{jD} is similar to that of C_{ds} and C_{gd} .

B. Loss Model Verification

(1) Switching waveform verification-By varying the magnitudes of the bus voltage and load inductance, the switching transient waveforms are obtained under different voltages and currents for theoretical calculations and experimental measurements, as shown in Fig 8.

In Fig 8, it can be seen that the model proposed in this paper agrees well with the experimental measurements at different voltages and currents. It can be seen that the model proposed in this paper matches well with experimental measurements at different voltages and currents, both for the turn-on process and the turn-off process and can reflect the SiC MOSFET switching transient waveform characteristics in a more detailed way.

(2) Switching loss verification-The accuracy of the loss calculation of the proposed model is verified by changing the external resistance $R_{G(ext)}$ of the drive circuit and the external gate-drain capacitance $C_{gd(ext)}$, respectively. The theoretical calculation results are compared with the experimentally measured results for $V_{DC}=400V$, $I_L=15A$, and the results are

TABLE III
PARAMETERS OF SiC MOSFET MODEL

Parameter	Value	Parameter	Value
C_L/pF	26	L_q/nH	6
V_{CC}/V	20	L_d/nH	150
V_{EE}/V	-5	g_{fs}/S	4.9
V_{miller}/V	9.66	C_{gs}/nF	2
C_{ds0}/nF	1.4	C_{gd0}/pF	571
C_{ds1}/pF	139	C_{gd1}/pF	15
C_{ds2}/pF	95	C_{gd2}/pF	11
V_{th}	5.9	$R_{G(int)}/\Omega$	5
C_{F0}/nF	1.2	v_{FO}/V	1.3
C_{F1}/pF	86	$R_{DS(on)}/m\Omega$	80
C_{F2}/nF	61	L_{SD}/nH	6.5
$R_{th1}^M(K/W)$	0.078	$C_{th1}^M(Ws/K)$	0.005
$R_{th2}^M(K/W)$	0.197	$C_{th2}^M(Ws/K)$	0.018
$R_{th3}^M(K/W)$	0.162	$C_{th3}^M(Ws/K)$	0.249
$R_{th1}^D(K/W)$	0.045	$C_{th1}^D(Ws/K)$	0.004
$R_{th2}^D(K/W)$	0.179	$C_{th2}^D(Ws/K)$	0.014
$R_{th3}^D(K/W)$	0.144	$C_{th3}^D(Ws/K)$	0.232

shown in Fig 9.

Fig. 9 (a) and (b) show the theoretical calculations and experimental measurements of the turn-off and turn-on losses for $R_G=10$, (c) and (d) show the comparison of the experimentally measured losses and the theoretically calculated losses for different R_G and different C_{gd} conditions.

From Fig. 9 (a) and (b), it can be seen that the turn-on loss is mainly generated in the current-rising stage and voltage-falling stage; the turn-off loss is mainly generated in the current-falling stage and voltage-rising stage. Although the theoretical waveform of this model does not match exactly with the experimental test in the oscillation phase, the oscillation phase has little effect on the turn-on loss and turn-off loss. Under different R_G and C_{gd} conditions, the total loss errors of the theoretical calculation and experiment are less than 6%, and the error comparison is shown in Table IV.

(3) parameters correction verification-Fig 10 (a) shows the

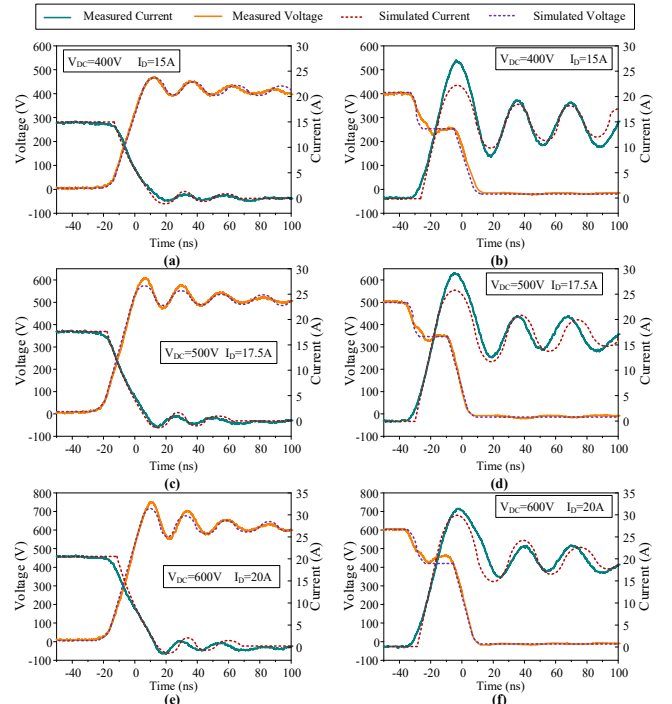


Fig. 8. Analytical calculation and experimental waveforms under different conditions.

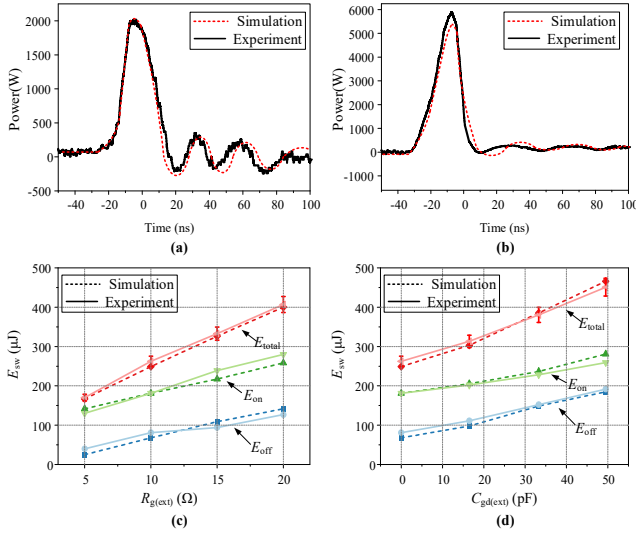


Fig. 9. Analytical calculation and experimental switching losses. (a) turn off loss waveform. (b) turn on loss waveform. (c) with different $R_{g(ext)}$. (d) with different $C_{gd(ext)}$

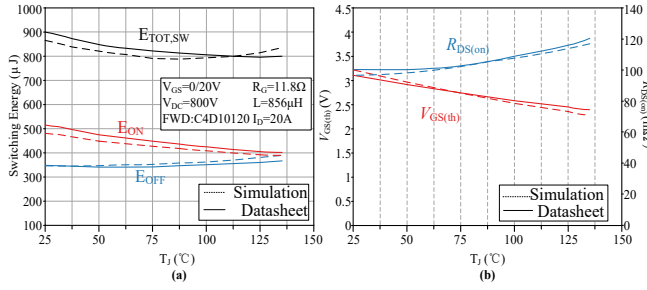


Fig. 10. (a) Simulate and datasheet switching energy versus junction temperature. (b) Simulate and datasheet parameters versus junction temperature.

simulation results of the switching energy of the SiC MOSFETs, which is obtained by simulating the switching energy of SiC MOSFETs at different temperatures to find the power loss of the device. Comparing the simulation results with the datasheet, it is found that the simulation data matches well with the datasheet at lower temperatures (about less than 100 °C), while the error increases at higher temperatures (more than 100 °C), and the high-temperature characteristics of the model need to

TABLE IV
COMPARISON OF EXPERIMENTAL LOSS AND SIMULATION LOSS

	R_g/Ω	5	10	15	20
Trun-on Loss	Experiment (μJ)	130.153	181.203	238.869	279.968
	Simulation (μJ)	141.779	181.195	217.300	258.384
	Error (%)	8.93%	0.00%	9.03%	7.71%
Trun-off Loss	Experiment (μJ)	40.078	81.162	94.023	126.792
	Simulation (μJ)	25.117	67.869	108.952	141.745
	Error (%)	37.33%	16.38%	15.88%	11.79%
Total Loss	Experiment (μJ)	170.231	262.365	332.892	406.76
	Simulation (μJ)	166.896	249.064	326.252	400.129
	Error (%)	1.96%	5.07%	1.99%	1.63%
	$C_{gd(ext)}/\text{pF}$	0	16.5	33.3	49.5
Trun-on Loss	Experiment (μJ)	181.195	202.066	228.177	259.273
	Simulation (μJ)	181.203	205.414	236.526	280.94
	Error (%)	0.00%	1.66%	3.66%	8.36%
Trun-off Loss	Experiment (μJ)	81.162	111.081	152.207	191.637
	Simulation (μJ)	67.869	97.778	148.859	184.97
	Error (%)	16.38%	11.98%	2.20%	3.48%
Total Loss	Experiment (μJ)	262.365	313.147	380.384	450.91
	Simulation (μJ)	249.064	303.192	385.385	465.91
	Error (%)	5.07%	3.18%	1.13%	3.33%

TABLE V
TEMPERATURE MEASURED TEST CONDITION

Parameter	Value	Parameter	Value
V_{DC}/V	400	R_L/Ω	5
$L_L/\mu\text{H}$	1000	$D(0s-2s)$	0.5
$D(2s-4s)$	0.4	$D(4s-6s)$	0.3
$D(6s-8s)$	0.4	$D(8s-10s)$	0.5
MOSFET	CMF20120D	SBD	C4D30120D

be improved. The simulation results also show that the effect of junction temperature on the switching loss is not significant, especially the turn-off switching loss does not change with the change of junction temperature. Fig 10 (b) shows the variation of temperature-related parameters of SiC MOSFET, which is consistent with the actual situation.

C. Thermal Model Verification

(1) Junction temperature verification-In this paper, FLUKE's Ti480 PRO thermal imager is used to measure the device temperature. The ambient temperature is 25 degrees Celsius. To demonstrate the accuracy of the temperature calculation, this paper creates a variety of test conditions by varying the duty cycle of the control signal. To ensure the accuracy of the temperature calculation measurements, the experiment was repeated five times in the same place using a thermal imager and averaged for smaller errors. The thermal image of SiC MOSFET and SiC SBD at 1s are shown in Fig 11, and the temperature measurement and thermal-level simulation are shown in Fig 12 (a).

The maximum error of the SiC MOSFET temperature is 3.2 degrees, and the relative error is 6.17%; the maximum error of the SBD temperature is 2.7 degrees, and the relative error is 6.87%. Modeling of thermal impedance is not the focus of this paper, further investigation is required.

(2) Data exchange step verification-Different data exchange steps can have an impact on the results of temperature calculation and parameter correction. Fig 12 (b) and (c) shows the temperature and step size using two different sizes of fixed steps and the variable step size proposed in this paper. If very small step sizes are used, e.g., 1e-5 s, the dynamics of the temperature change process can be simulated very finely. Conversely, a large number of computational resources are required for calculating the loss power and temperature corrections. If a very large step size is used, e.g., 1e-2 s, the computational effort to update the loss power and temperature corrections can be greatly reduced. However, the calculated temperature differs significantly from that using a small step size (1e-5 s).

The adaptive step size proposed in this paper can compromise the accuracy of temperature calculation and the consumption of computational resources. As can be seen in Fig 12 (b), although the step size is much larger than the fixed step size (1e-5 s), the accuracy is already very close, with a maximum error of 2 degrees Celsius. From Fig 12 (c), it can be seen that for a simulation of 0.1s, if a fixed step size (1e-5 s) is used, the data needs to be updated 1000 times, while the adaptive step size only needs to be updated 26 times. Thermal simulations are often at the minute level or even longer, this adaptive data exchange method can greatly save computational

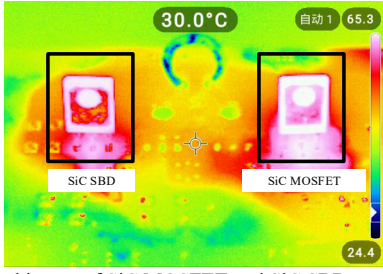


Fig. 11. Thermal image of SiC MOSFET and SiC SBD

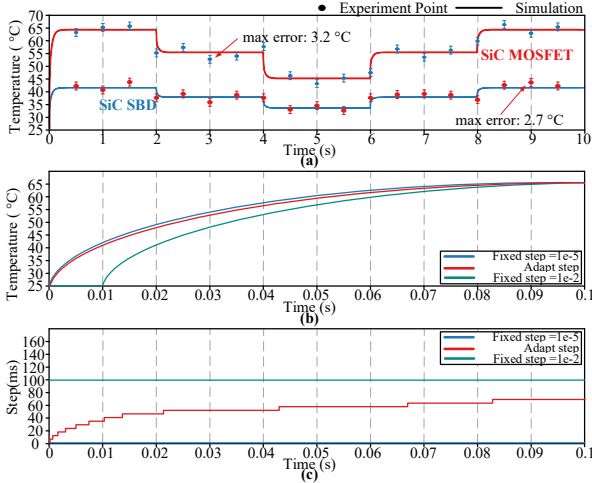


Fig. 12. Analytical calculation and experimental device temperature. Comparison of MOSFET case temperature using different data exchange step. (a) Temperature. (b) Step size.

resources while ensuring computational accuracy subsequently.

VI. CONCLUSION

In this paper, a transient time-segmented loss model for SiC power switching devices is proposed, which can be used for the simulation of the switching transients, power losses and device junction temperatures of SiC MOSFETs.

1. In this paper, a transient time-segmented loss model based on SiC MOSFET and SiC SBD switching pair is established. The model has considered the impact of displacement current which cannot be neglected when the drain current is low. The model also considers the impact of nonlinear parameters, such as the junction capacitances, the temperature-related parameters, and the oscillation phenomenon caused by stray parameters.

2. The proposed losses model can also calculate the transient waveform and characterize the switching transients of SiC MOSFETs in more details compared with other behavior model of SiC MOSFET. The model parameters can be extracted from the datasheet, which has strong practicality. This model requires only external conditions: bus voltage and load current, and can be applied in all kinds of system-level simulation method with generality.

3. The proposed loss model can also be used in junction temperature calculation. The loss model and thermal network model are used in system-level simulation to compose an electro-thermal simulation platform. And the strategy is

proposed where the adaptive data interaction step can greatly save the computational resources while ensuring computational accuracy.

APPENDIX DERIVATIONS OF SWITCHING PROCESS

A. Turn-on Analysis

Stage 2 (t_2 - t_3): v_{gs} increases to $V_{gs}(t_3)$ at t_3 , which is expressed as

$$V_{gs}(t_3) = \frac{I_L}{2g_{fs}} + V_{th}. \quad (25)$$

Meanwhile, v_{ds} decreases to V_{ds0} and the difference between V_{ds0} and V_{ds} is V_{drop} . V_{ds0} and V_{drop} are expressed as

$$V_{ds0} = V_{DC} + v_F - V_{drop} = V_{DC} + v_F - L_{stray} \frac{I_L}{2(t_3 - t_2)}. \quad (26)$$

Stage 3 (t_3 - t_4): v_{gs} increases to V_{miller} at t_4 when $i_d = I_L$, V_{miller} is

$$V_{miller} = \frac{I_L}{g_{fs}} + V_{th}. \quad (27)$$

Stage 4 (t_4 - t_5): Due to SBD capacitance discharging at this stage, i_d increases from I_L and reaches to I_{peak} at t_5 . I_{peak} is

$$I_{peak} = I_L + \frac{2C_{F(eq)}(V_{DC} + v_F - V_{ds0})}{t_5 - t_4}. \quad (28)$$

According to (8), V_{gs_peak} is

$$V_{gs_peak} = \frac{I_{peak}}{g_{fs}} + V_{th}. \quad (29)$$

Stage 6 (t_6 - t_7): the SiC MOSFET is in the saturation region at this stage. $V_{ds(on)}$ is

$$V_{ds(on)} = I_L R_{ds(on)}. \quad (30)$$

B. Turn-off Analysis

Stage 3 (t_3 - t_4): i_d increases to I_{t4} at t_4 . I_{t4} is expressed using (14) as

$$I_{t4} = I_L - C_{F(eq)} \frac{\Delta V_{ds1}}{t_4 - t_3}. \quad (31)$$

According to (8), $V_{gs}(t_6)$ is

$$V_{gs}(t_6) = \frac{1}{g_{fs}} \left(I_{t6} - C_{oss} \frac{\Delta V_{ds3}}{t_6 - t_5} \right) + V_{th}. \quad (32)$$

Stage 4 (t_4 - t_5): v_{ds} increases to V_{peak} at t_7 . V_{peak} is expressed as

$$V_{peak} = V_{DC} + v_{F0} + L_{stray} I_{t6} / (t_7 - t_6). \quad (33)$$

REFERENCES

- [1] "Fabrication and Characterization of a High-Power-Density, Planar 10 kV SiC MOSFET Power Module | VDE Conference Publication | IEEE Xplore." <https://ieeexplore.ieee.org/document/8403187> (accessed Jun. 10, 2021).
- [2] T. Ishigaki *et al.*, "A 3.3 kV / 800 A Ultra-High Power Density SiC Power Module," in *PCIM Europe 2018; International Exhibition and Conference for Power Electronics, Intelligent Motion, Renewable Energy and Energy Management*, Jun. 2018, pp. 1–5.
- [3] L. Zhang *et al.*, "Performance Evaluation of High-Power SiC MOSFET Modules in Comparison to Si IGBT Modules," *IEEE Trans. Power Electron.*, vol. 34, no. 2, pp. 1181–1196, Feb. 2019.

- [4] T. Zhao *et al.*, “Comparisons of SiC MOSFET and Si IGBT Based Motor Drive Systems,” in *2007 IEEE Industry Applications Annual Meeting*, Sep. 2007, pp. 331–335.
- [5] H. Mirzaee *et al.*, “Design Comparison of High-Power Medium-Voltage Converters Based on a 6.5-kV Si-IGBT/Si-PiN Diode, a 6.5-kV Si-IGBT/SiC-JBS Diode, and a 10-kV SiC-MOSFET/SiC-JBS Diode,” *IEEE Trans. Ind. Appl.*, vol. 50, no. 4, pp. 2728–2740, Jul. 2014.
- [6] J. Zheng *et al.*, “An Event-Driven Real-Time Simulation for Power Electronics Systems Based on Discrete Hybrid Time-Step Algorithm,” *IEEE Trans. Ind. Electron.*, vol. 70, no. 5, pp. 4809–4819, May 2023.
- [7] J. Zheng *et al.*, “An Event-Driven Parallel Acceleration Real-Time Simulation for Power Electronic Systems Without Simulation Distortion in Circuit Partitioning,” *IEEE Trans. Power Electron.*, vol. 37, no. 12, pp. 15626–15640, Dec. 2022.
- [8] J. Zheng *et al.*, “A Semi-implicit Parallel Leapfrog Solver with Half-Step Sampling Technique for FPGA-based Real-time HIL Simulation of Power Converters,” *IEEE Trans. Ind. Electron.*, pp. 1–10, 2023.
- [9] J. Zheng *et al.*, “MPSoC-Based Dynamic Adjustable Time-Stepping Scheme with Switch Event Oversampling Technique for Real-time HIL Simulation of Power Converters,” *IEEE Trans. Transp. Electrification*, pp. 1–1, 2023.
- [10] J. Zheng *et al.*, “An Event Driven Synchronization Framework for Physical Controller Co-Simulation of Megawatt-level Power Electronic Systems,” *IEEE Trans. Ind. Electron.*
- [11] F. Wagner *et al.*, “Power Cycling of SiC-MOSFET Single-Chip Modules with Additional Measurement Cycles for Life End Determination,” in *CIPS 2020; 11th International Conference on Integrated Power Electronics Systems*, Mar. 2020, pp. 1–6.
- [12] J. Wang *et al.*, “A Data-based IGBT Model for Efficient and Accurate Electro-thermal Analysis,” in *2020 IEEE Energy Conversion Congress and Exposition (ECCE)*, Oct. 2020, pp. 3442–3448.
- [13] T. Langbauer *et al.*, “Closing the Loop between Circuit and Thermal Simulation: A System Level Co-Simulation for Loss Related Electro-Thermal Interactions,” p. 6, 2019.
- [14] D. Jiang *et al.*, “Temperature-Dependent Characteristics of SiC Devices: Performance Evaluation and Loss Calculation,” *IEEE Trans. Power Electron.*, vol. 27, no. 2, pp. 1013–1024, Feb. 2012.
- [15] T. R. McNutt *et al.*, “Silicon Carbide Power MOSFET Model and Parameter Extraction Sequence,” *IEEE Trans. Power Electron.*, vol. 22, no. 2, pp. 353–363, Mar. 2007.
- [16] Y. Xiao *et al.*, “Corner and Statistical SPICE Model Generation for Shielded-Gate Trench Power MOSFETs Based on Backward Propagation of Variance,” in *2019 IEEE Applied Power Electronics Conference and Exposition (APEC)*, Mar. 2019, pp. 508–515.
- [17] J. Wang *et al.*, “Characterization and Experimental Assessment of the Effects of Parasitic Elements on the MOSFET Switching Performance,” *IEEE Trans. Power Electron.*, vol. 28, no. 1, pp. 573–590, Jan. 2013.
- [18] K. Peng *et al.*, “Analytical loss model for power converters with SiC MOSFET and SiC schottky diode pair,” in *2015 IEEE Energy Conversion Congress and Exposition (ECCE)*, Sep. 2015, pp. 6153–6160.
- [19] R. Wu *et al.*, “A Temperature-Dependent Thermal Model of IGBT Modules Suitable for Circuit-Level Simulations,” *IEEE Trans. Ind. Appl.*, vol. 52, no. 4, p. 9, 2016.
- [20] R. Cao *et al.*, “Thermal Modeling of Power Semiconductor Devices with Heat Sink Considering Ambient Temperature Dynamics,” in *2020 IEEE 9th International Power Electronics and Motion Control Conference (IPEMC2020-ECCE Asia)*, Nanjing, China, Nov. 2020, pp. 290–295.
- [21] H. Bai *et al.*, “An FPGA-Based IGBT Behavioral Model With High Transient Resolution for Real-Time Simulation of Power Electronic Circuits,” *IEEE Trans. Ind. Electron.*, vol. 66, no. 8, pp. 6581–6591, Aug. 2019.
- [22] H. Bai *et al.*, “FPGA-Based Device-Level Electro-Thermal Modeling of Floating Interleaved Boost Converter for Fuel Cell Hardware-in-the-Loop Applications,” *IEEE Trans. Ind. Appl.*, vol. 55, no. 5, pp. 5300–5310, Sep. 2019.
- [23] Z. Shen *et al.*, “Real-Time Device-Level Transient Electrothermal Model for Modular Multilevel Converter on FPGA,” *IEEE Trans. Power Electron.*, vol. 31, no. 9, pp. 6155–6168, Sep. 2016.
- [24] C. Batard *et al.*, “Lumped Dynamic Electrothermal Model of IGBT Module of Inverters,” *IEEE Trans. Compon. Packag. Manuf. Technol.*, vol. 5, no. 3, pp. 355–364, Mar. 2015.
- [25] B. Shi *et al.*, “Piecewise Analytical Transient Model for Power Switching Device Commutation Unit,” *IEEE Trans. Power Electron.*, vol. 34, no. 6, pp. 5720–5736, Jun. 2019.
- [26] I. Castro *et al.*, “Analytical Switching Loss Model for Superjunction MOSFET With Capacitive Nonlinearities and Displacement Currents for DC–DC Power Converters,” *IEEE Trans. Power Electron.*, vol. 31, no. 3, pp. 2485–2495, Mar. 2016.
- [27] “SiC MOSFET N-Ch Enhancement CMF20120D Z-FET | Wolfspeed.” <https://www.wolfspeed.com/cm20120d> (accessed Jun. 11, 2021).
- [28] “Discrete SiC Schottky Diodes 1200V | Power | Wolfspeed.” <https://www.wolfspeed.com/1200v-silicon-carbide-schottky-diodes> (accessed Jun. 11, 2021).



Jialin Zheng. (Student Member, IEEE) received the B.S. degree in electrical engineering in 2019 from Beijing Jiaotong University, Beijing, China. Since 2019, he has been working toward the Ph.D. degree in electrical engineering at the Department of Electrical Engineering, Tsinghua University, Beijing, China. His research interests include real-time simulation, in power electronics.



Zhengming Zhao (Fellow, IEEE) received the B.S. and M.S. degrees in electrical engineering from Hunan University, Changsha, China, in 1982 and 1985, respectively, and the Ph.D. degree in electrical engineering from Tsinghua University, Beijing, China, in 1991. He is currently a Professor with the Department of Electrical Engineering, Tsinghua University. His research interests include high-power conversion, power electronics and motor control.



Han Xu (Student member, IEEE) received the B.S. degree in electrical engineering in 2021 from Tsinghua University, Beijing, China. Since 2021, he has been working toward the master degree in electrical engineering at the Department of Electrical Engineering, Tsinghua University, Beijing, China. His research interests include simulation of power electronic systems.



Weicheng Liu (Student member, IEEE) received the B. E. degree in electrical engineering from Southeast University, China, in 2018, and M.S degree in electrical engineering from Southeast University in 2021. He is currently working towards the Ph.D. degree in electrical engineering from Tsinghua University, China. His current research interests include power system simulation methodology and technique.



Yangbin Zeng (Member, IEEE) received the B.Sc. degree in Building Electrical and Intelligent from Xiangtan University, Xiangtan, China, in 2015, the Ph.D. degree in electrical engineering from Beijing Jiaotong University, Beijing, China, in 2021. Now, he is a postdoctoral researcher in Department of Electrical Engineering, Tsinghua University, Beijing. His current research interests include real-time simulation.